Check for updates

How to cite: *Angew. Chem. Int. Ed.* **2023,** *62,* e202218555
International Edition: doi.org/10.1002/anie.202218555
German Edition: doi.org/10.1002/ange.202218555

Supramolecular Polymers

Anticooperative Supramolecular Oligomerization Mediated by V-Shaped Monomer Design and Unconventional Hydrogen Bonds

Beatriz Matarranz[+], Sandra Díaz-Cabrera[+], Goutam Ghosh, Israel Carreira-Barral, Bartolome Soberats, María García-Valverde, Roberto Quesada,* and Gustavo Fernández**

Abstract: After more than three decades of extensive investigations on supramolecular polymers, strategies for self-limiting growth still remain challenging. Herein, we exploit a new V-shaped monomer design to achieve anticooperatively formed oligomers with superior robustness and high luminescence. In toluene, the monomer-oligomer equilibrium is shifted to the monomer side, enabling the elucidation of the molecular packing modes and the resulting (weak) anticooperativity. Steric effects associated with an antiparallel staircase organization of the dyes are proposed to outcompete aromatic and unconventional B–F···H–N/C interactions, restricting the growth at the stage of oligomers. In methylcyclohexane (MCH), the packing modes and the anticooperativity are preserved; however, pronounced solvophobic and chain-enwrapping effects lead to thermally ultrastable oligomers. Our results shed light on understanding anticooperative effects and restricted growth in self-assembly.

Introduction

Molecular self-assembly is a powerful tool to create supramolecular architectures with precise morphologies and functionalities.[1] Particularly successful tactics in this regard harness the inherent potential of π-conjugated scaffolds to undergo aromatic interactions,[2] often combined with directional non-covalent forces, such as hydrogen (H−) bonding, to further enhance the assembly stability.[3] In fact, this combination of interactions is included in nearly each monomer design for supramolecular polymerization, as their orthogonality and strength readily enables one-dimensional cooperative growth and high order.[4] However, as a result of these characteristics, it is challenging to limit the assembly process,[5] which explains why examples of size-restricted anticooperative growth remain scarce.

Because in anticooperative supramolecular polymerizations nucleation is favored over elongation,[6] monomer design strategies should fulfil a fundamental requirement: the competition of different non-covalent interactions should allow the stabilization of particularly stable nuclei,[7] and/or the destabilization of the subsequent elongation step, typically building increasing steric effects[8] or charge repulsion.[9] While these notions are already established in the literature, implementing them successfully is far from trivial: if steric or charge repulsion becomes too dominant, self-assembly may be either inhibited,[10] or, in some cases, a molecular rearrangement may entirely change the aggregation mechanism and the outcome of the system.[11] Hence, considerable research efforts are necessary to establish general design guidelines for size-limited anticooperative assemblies.

Strikingly, most examples of anticooperative assemblies bear a preorganized and/or undistorted (π-extended) aromatic core—anticooperativity is then largely governed by the substituents and side groups.[7–9] In an attempt to broaden the monomer scope for anticooperative self-assembly, we reasoned that the reduction of the aromatic core's preorganization might hinder effective aromatic interactions, thereby limiting the growth upon self-assembly. We thus designed a BODIPY dye with extended phenylethynyl substituents at the 3- and 5-positions, which provide the system with a non-preorganized V-shaped molecular geometry (**1** in Scheme 1). Amide groups and alkyl side chains were further included in the design in order to enable attractive forces (H-bonding) and maintain solubility in non-

[*] Dr. B. Matarranz,[+] Dr. G. Ghosh, Prof. Dr. G. Fernández
Westfälische Wilhelms-Universität Münster, Organisch-Chemisches Institut
Corrensstraße 36, 48149 Münster (Germany)
E-mail: fernandg@uni-muenster.de
Dr. S. Díaz-Cabrera,[+] Dr. I. Carreira-Barral,
Prof. Dr. M. García-Valverde, Prof. Dr. R. Quesada
Departamento de Química, Facultad de Ciencias, Universidad de Burgos
09001 Burgos (Spain)
E-mail: magaval@ubu.es
rquesada@ubu.es
Dr. B. Soberats
Department of Chemistry, Universitat de les Illes Balears
Cra. Valldemossa, Km. 7.5, 07122 Palma de Mallorca (Spain)
[+] co-first authors

© 2023 The Authors. Angewandte Chemie International Edition published by Wiley-VCH GmbH. This is an open access article under the terms of the Creative Commons Attribution Non-Commercial License, which permits use, distribution and reproduction in any medium, provided the original work is properly cited and is not used for commercial purposes.

© 2023 The Authors. Angewandte Chemie International Edition published by Wiley-VCH GmbH

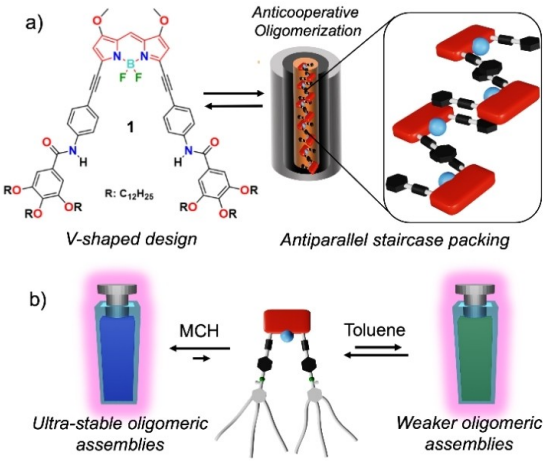

Scheme 1. Chemical structure of BODIPY **1** and schematic representation of its anticooperative supramolecular oligomerization and molecular packing.

polar media, respectively. The incorporation of methoxy groups at the 1- and 7-positions of the BODIPY is inspired by the intriguing optical and biological properties of the prodigiosin alkaloid family.[12] Additionally, three V-shaped BODIPYs with either an ester (**2**) or an alkyne linkage (**3**) instead of an amide, or with methoxy groups (**4**) instead of dodecyloxy keeping the amide linker, were used as control molecules to examine potential packing effects and H-bonding (synthesis & characterization of **1**–**4** are shown in the Supporting Information).

We found that the selected structural elements of **1** not only induce an attenuated anticooperative growth into highly luminescent oligomer stacks of 13–24 BODIPY units, but they also shift the absorption and emission properties closer to the NIR region compared to parent BODIPY dyes.[13] We propose that increasing steric effects associated with an inefficient antiparallel packing along with chain enwrapping effects counterbalance the existing attractive unconventional B–F···H–N/C intermolecular interactions, leading to a self-limiting growth. Notably, the oligomers exhibit a unique, ultrahigh thermal stability in methylcyclohexane (MCH), which is an uncommon property of anticooperative assemblies. Our results shed light on the previously elusive aggregation of V-shaped monomers and broaden the scope of anticooperative self-assembly.

Results and Discussion

Self-Assembly of 1

Solvent-dependent UV/Vis and emission studies (Figure S1) allowed us to identify three different trends in the spectroscopic behavior of **1** at μM concentrations. We selected tetrahydrofuran (THF), toluene and MCH as representative solvents describing each trend, while for a more detailed discussion of the spectroscopic studies in various solvents, the reader is referred to the Supporting Information. In relatively polar THF, the absorption spectrum shows a sharp, intense BODIPY $S_0 \rightarrow S_1$ transition at 615 nm (Figure 1), which is typical for molecularly dissolved BODIPYs (trend I).[13] This $S_0 \rightarrow S_1$ transition also displays a vibronic pattern with two additional shoulder bands at ca. 540 and 570 nm (Figure 1). A second transition at ca. 360 nm, assigned to the large aromatic substituents of the BODIPY, is also visible, which overlaps with the BODIPY $S_0 \rightarrow S_2$ transition in the region between ca. 380–460 nm. On the other hand, when the driving force for self-assembly is increased using an aromatic non-polar solvent as toluene, the intensity of the absorption maximum nearly halves and the maximum slightly red-shifts to 619 nm ($\Delta\lambda = 4$ nm). In addition, a red-shifted shoulder band at 644 nm develops (trend II, Figure 1). Besides, the transition at 350 nm slightly decreases in intensity compared to THF, and simultaneously the absorption between ca. 400–500 nm increases. The spectral changes in toluene point to some sort of self-assembled structure that develops upon decreasing the solvent polarity. Finally, if the solvent polarity is further reduced (MCH), the overall absorption intensity further drops, and the shoulder at 644 nm observed in toluene develops as a more intense, sharp transition (Figure 1). Moreover, a second, blue-shifted absorption maxima at 593 nm emerges alongside the main absorption at 611 nm, indicating shorter intermolecular distances between the chromophores in MCH compared to toluene (trend III). The three trends observed in absorption studies are likewise distinguishable in emission studies. In THF, the emission spectrum of **1** displays a maximum at 635 nm and a shoulder at 690 nm, with a Stokes shift of 19 nm (Figure 1). This maximum is also visible in toluene, but coexists with an additional red-shifted emission band of higher intensity at 661 nm (Figure 1). In MCH, this red-shifted emission becomes the only observable band, which appears alongside an additional shoulder at 721 nm (Figure 1). The absence of the emission band at ca. 635 nm in MCH indicates a more efficient aggregation in MCH compared to toluene. Also, the relatively large Stokes shift in MCH (51 nm) compared to the monomer in THF (19 nm) could be attributable to a weak exciton coupling between BODIPY dyes rather than to *J*-type aggregation.[14] Excitation spectra in toluene at

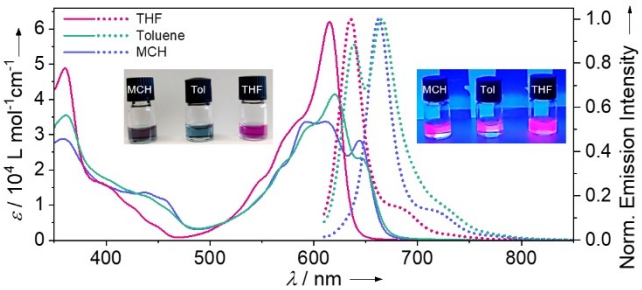

Figure 1. Solvent-dependent UV/Vis (solid lines) and fluorescence (dotted lines) spectra of BODIPY **1** ($c = 10$ μM, $\lambda_{exc} = 600$ nm, 298 K) and photographs of the solutions in MCH, toluene and THF under daylight (inset, left) and under UV/Vis irradiation (inset, right).

© 2023 The Authors. Angewandte Chemie International Edition published by Wiley-VCH GmbH

15213773, 2023, 17, Downloaded from https://onlinelibrary.wiley.com/doi/10.1002/anie.202218555 by Universidad De Burgos, Wiley Online Library on [07/02/2024]. See the Terms and Conditions (https://onlinelibrary.wiley.com/terms-and-conditions) on Wiley Online Library for rules of use; OA articles are governed by the applicable Creative Commons License

room temperature showed the typical spectral patterns of monomeric (collected at 640 nm) and aggregated **1** (collected at 665 nm), suggesting an equilibrium between these two species (Figure S5). Interestingly, the fluorescence quantum yield (Φ_f) of **1** was found to be high both in the molecularly dissolved state in THF (0.93) and in the aggregated state ($\approx$0.59 for both toluene and MCH; Table S1). These remarkable Φ_f values for aggregated species may result from weak exciton coupling, i.e., lack of short dye-dye interactions in the self-assembled state. Note that BODIPYs **2** and **3** (with an ester or alkyne linker, respectively) show no or negligible aggregation in toluene and MCH under similar conditions (Figures S23–S29), suggesting that the amide groups of **1** play an important role in the observed self-assembly.

Mechanistic and morphological insights into the self-assembly of 1 in toluene and MCH

To gain mechanistic insights into the self-assembly process both in toluene and MCH, we employed variable temperature (VT), variable concentration (VC) and denaturation studies. VT-UV/Vis studies of **1** (c = 10 μM) in MCH show nearly no changes upon heating to 353 K, even after keeping the solution at this temperature over time (Figure S6), indicating that the aggregates in MCH have a very high thermal stability under these conditions. Decreasing the concentration to 2.5 μM also resulted in no complete disassembly at high temperature, but rather in an absorption spectrum that resembles that obtained in toluene at room temperature (Figure S9). The incomplete dissociation of the aggregates in MCH is also observed in VT-emission studies (Figure S10). In toluene, on the other hand, thermal annealing efficiently dissociates the aggregates and progressively forms the typical spectral pattern of monomeric **1** at high temperatures (Figure 2a). Subsequent cooling to 263 K results in a decrease of the absorption maximum at 611 nm, accompanied by a slight blue-shift to 618 nm and the concomitant appearance of a red-shifted shoulder at 646 nm. These spectroscopic features indicate a reversible transition from the molecularly dissolved to the aggregated species, which is accompanied by a change in color from pink to bluish violet (Figure 2d, inset). It should be stressed that no defined isosbestic points are observed in these studies, suggesting the absence of a clear equilibrium between the monomer and a defined species such as a dimer. The corresponding cooling curves at 646 nm displayed a sigmoidal shape and were thus fitted to the isodesmic model (Figure 2d, Table S2).[15] However, some deviations from a perfect sigmoidal curve were observed, especially at high and low α_{agg} values, suggesting the existence of an anti-cooperative mechanism.[6]

Subsequent UV/Vis denaturation studies in toluene using THF as denaturing agent were unsuccessful, as the aggregates of **1** in toluene are extremely sensitive to the addition of minor amounts of monomeric **1** in THF (Figure S13). Nevertheless, these experiments were successful in MCH, where we previously demonstrated a much higher aggregate thermal stability than in toluene. In these studies,

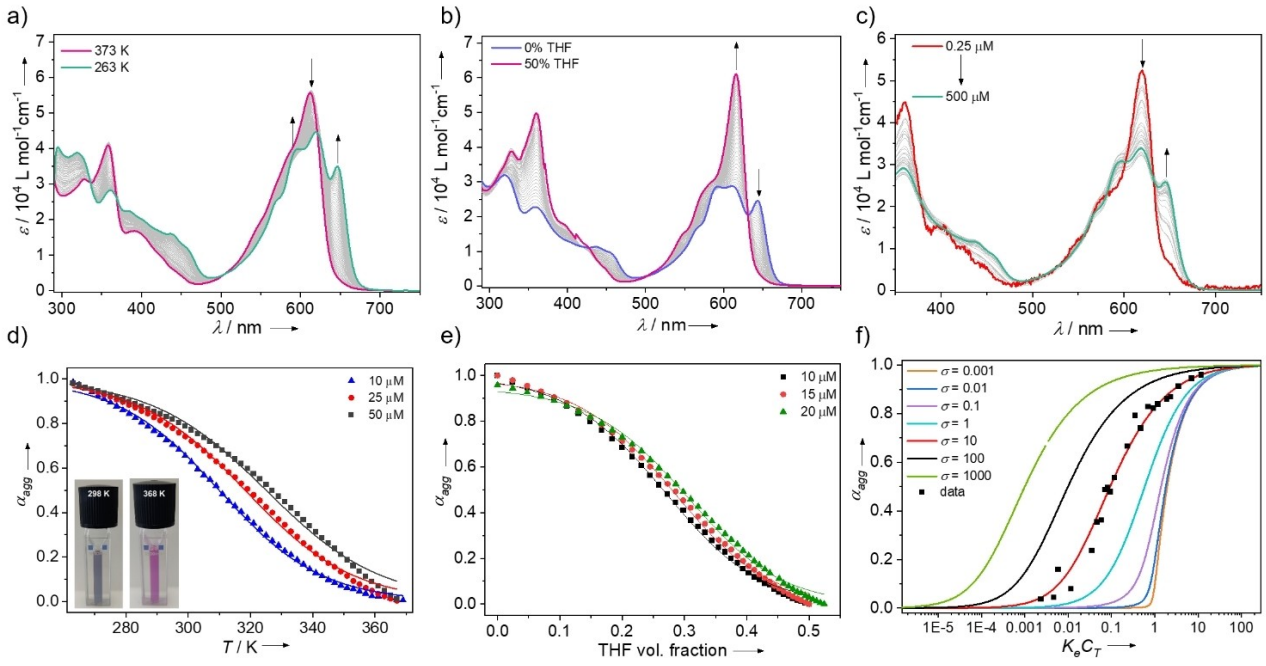

Figure 2. a) VT-UV/Vis spectra of **1** in toluene (c = 25 μM, cooling rate: 1 K/min) and d) the corresponding fitting of the cooling curves at 646 nm to the isodesmic mechanism; b) denaturation UV/Vis studies of **1** in MCH/THF (c = 10 μM, T = 298 K) and e) the corresponding fitting of the denaturation curves to the denaturation model obtained in MCH/THF at 645 nm; c) concentration-dependent UV/Vis spectra of **1** in toluene (T = 298 K) and f) the corresponding fit to the Goldstein-Styer model (σ = 10).

© 2023 The Authors. Angewandte Chemie International Edition published by Wiley-VCH GmbH

15213773, 2023, 17, Downloaded from https://onlinelibrary.wiley.com/doi/10.1002/anie.202218555 by Universidad De Burgos, Wiley Online Library on [07/02/2024]. See the Terms and Conditions (https://onlinelibrary.wiley.com/terms-and-conditions) on Wiley Online Library for rules of use; OA articles are governed by the applicable Creative Commons License

the stepwise addition of monomeric **1** in THF to aggregated **1** in MCH at the same concentration (between 10 and 20 μM) results in the full transformation of the aggregated species into the monomer when the THF content exceeds 50 % (Figure 2b). The plots of α_{agg} vs. the volume fraction of THF afford sigmoidal curves for three different concentrations (Figure 2e). However, fitting of these data using the denaturation model[16] results in discrepancies at both high and low α_{agg} values, in a similar manner as it was observed in toluene in VT-UV/Vis. Therefore, the self-assembly process of **1** both in toluene and MCH cannot be precisely described by the isodesmic model, neither in VT (in toluene) nor in denaturation studies (in MCH).

Considering the lack of thermodynamic models that are able to describe anticooperative supramolecular polymerizations in temperature- and solvent-dependent experiments, we monitored the changes in absorption of **1** in toluene and MCH vs. concentration in order to apply the Goldstein-Stryer K_2-K model.[17] As expected, the high stability of the aggregates in MCH is also obvious in VC-UV/Vis studies, wherein nearly no changes in the spectral pattern are observed upon diluting the sample from 1 mM to 1 μM (Figure S3). This behavior is dramatically different in toluene: upon dilution from 0.5 mM to 0.25 μM, the intensity of both the red-shifted band at 644 nm and that of the shoulder at 595 nm gradually decreases at the expense of the typical monomeric absorption at 611 nm (Figure 2c). These spectral changes disclose a gradual disassembly process upon dilution, although the fact that the shoulder at 644 nm is still visible to a minor extent at the lowest measurable concentration (0.25 μM) indicates that the disassembly process is nearly but not entirely complete. We analyzed the spectral changes as a function of concentration with the Goldstein-Stryer model (α_{agg} vs. $K\times c$) and found that the resulting plot is best reproduced using a σ value of 10 (Figure 2f), in agreement with a weakly anticooperative process (for comparison, the fits using σ values of 1 (isodesmic) and 100 (more anticooperative) are shown in Figure S15). Note that the dimer model[7d] does not accurately reproduce the experimental VC data (Figure S15). Even though the high association constant of **1** precluded us to cover the whole disassembly curve (at $\alpha_{agg} < 0.1$, we were below the detection limit of the spectrometer), the upper region of the curve clearly deviates from an isodesmic process ($\sigma = 1$, see Figure S15).

Thus, we can conclude on the basis of the curve shapes of three independent set of experiments (VT-, solvent-dependent and VC-UV/Vis) that an anticooperative mechanism is the most plausible process accounting for the self-assembly of **1**. The presence of discrete aggregates observed in atomic force microscopy (AFM) studies (Figure S21) also agrees with this hypothesis.

Further proof for an anticooperative self-assembly was provided by small-angle X-ray scattering (SAXS) experiments. Figure 3 shows the SAXS profiles for compound **1** ($c = 2$ and 4×10^{-3} M, 298 K) in toluene and MCH (Figure 3a,b). The SAXS profiles reveal nearly no q^{-1} slope, which indicates the formation of small discrete aggregates and therefore rule out the presence of highly anisotropic one-dimensional assemblies. The experimental curves were fitted to different customized models, including rigid cylinders, elliptical cylinders and spheres, and we obtained the best fits using the cylinder customized model (Figure 3 and Table S4,5). The fits indicate that compound **1** self-assembles into small cylinder morphologies with lengths of 75–85 Å and 45–85 Å in MCH and toluene, respectively. These cylinder lengths are consistent with the formation of stacks of 13–24 BODIPYs. The small size of these assemblies was further confirmed by ^{1}H DOSY NMR revealing the presence of aggregated species with hydrodynamic radii of ca. 17 Å in MCH (Figure S22). These results confirm the formation of discrete oligomer stacks that are characteristic of an anticooperative self-assembly process.

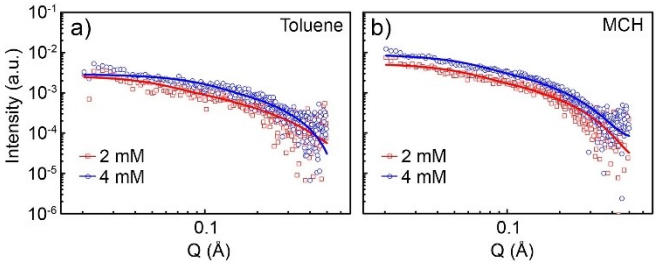

Figure 3. SAXS profiles (circles) for the assemblies formed by **1** in toluene (a) and MCH (b) at ca. 2 mM (red) and ca. 4 mM (blue) and the corresponding fittings (solid lines) to the customized cylinder model.

Elucidation of the non-covalent interactions and packing modes

In order to shed light on the non-covalent interactions that govern the self-assembly of **1** in MCH and toluene and the resulting molecular packing, Fourier-transform infrared spectroscopy (FTIR) experiments were initially performed (Figure S16). The amide N-H stretching frequencies (3387 and 3390 cm^{-1} for MCH and toluene, respectively) are lower than typical values of non-bonded amides (ca. 3430 cm^{-1}),[8b,18b] but considerably higher than those observed in systems engaged in typical amide-amide C=O···H–N H-bonds,[18] which suggests the formation of other, less conventional and weaker H-bonds.[18b,19] On the other hand, the values of carbonyl stretching (1683 and 1679 cm^{-1} for MCH and toluene, respectively, Figure S16) agree with the presence of free, non-H-bonded C=O groups.[20] On the basis of these results, we conclude that only the N–H groups, but not the C=O groups of the amides are engaged in (weak) H-bonding in toluene and MCH. Given that compound **1** bears various other heteroatoms that can potentially act as H-bonding acceptors to bind the amide N–H groups (the peripheral dodecyloxy oxygens, the methoxy oxygens or the fluorine atoms bonded to the boron centre[21]), these possibilities were explored using a wide range of 1D and 2D NMR methods.

The good signal resolution of **1** in toluene-d_8 at mM concentration allowed us to perform VT-^{1}H-NMR experi-

© 2023 The Authors. Angewandte Chemie International Edition published by Wiley-VCH GmbH

15213773, 2023, 17, Downloaded from https://onlinelibrary.wiley.com/doi/10.1002/anie.202218555 by Universidad De Burgos, Wiley Online Library on [07/02/2024]. See the Terms and Conditions (https://onlinelibrary.wiley.com/terms-and-conditions) on Wiley Online Library for rules of use; OA articles are governed by the applicable Creative Commons License

ments (Figure 4a). Upon cooling from 363 K to 283 K, the signal of the amide N–H groups (red) shifts downfield, suggesting the formation of H-bonding interactions. A similar yet slightly less pronounced downfield shift is observed for the resonances of the *p*-substituted aromatic ring (blue) that are located in *ortho*-position with respect to the amide N–H. In contrast, the adjacent position (the aromatic C–H groups in *meta*-position with respect to the amide N–H, light blue) remains nearly unaffected upon cooling. Given the similar trends experienced by the resonances of the amide N–H (red) and its adjacent C–H in *ortho* (dark blue), both groups are possibly located in the vicinity of the same heteroatom as H-bonding acceptor, being the distance N–H···X(heteroatom) shorter than the distance C–H···X(heteroatom). Additionally, the fact that the C–H groups in *meta*-position with respect to the amide N–H (light blue) negligibly shift, rules out the involvement of this aromatic ring in π-stacking interactions. On the other hand, the proton signals corresponding to the hydrogens at the 2- and 6-positions of the BODIPY core (pink) undergo nearly no shifts, revealing weak intermolecular interactions of the BODIPY cores upon aggregation, in agreement with the lack of strong exciton coupling observed in spectroscopic experiments. With regards to the dodecyloxy side chains, while the signals of the inner (*para*) O–C$\underline{H}_2$ groups remain invariant (light green), the protons of the outer (*meta*) O–C$\underline{H}_2$ groups shift upfield upon cooling (dark green). These results suggest that the O–C$\underline{H}_2$ groups of the outer chains are located in a more electron-rich environment. Interestingly, the signals of the methoxy hydrogens at the 1- and 7-positions of the BODIPY core undergo a marked downfield shift upon cooling (purple), suggesting the proximity of an H-bonding acceptor, i.e., a heteroatom.

The opposed trends of the O–C$\underline{H}_2$ outer (dark green) vs. O–C$\underline{H}_3$ BODIPY protons (purple) may indicate that these signals are interrelated. The absence of signal broadening in the course of the VT-^{1}H-NMR experiments rules out the formation of extended anisotropic assemblies,[22] as previously proposed by SAXS.

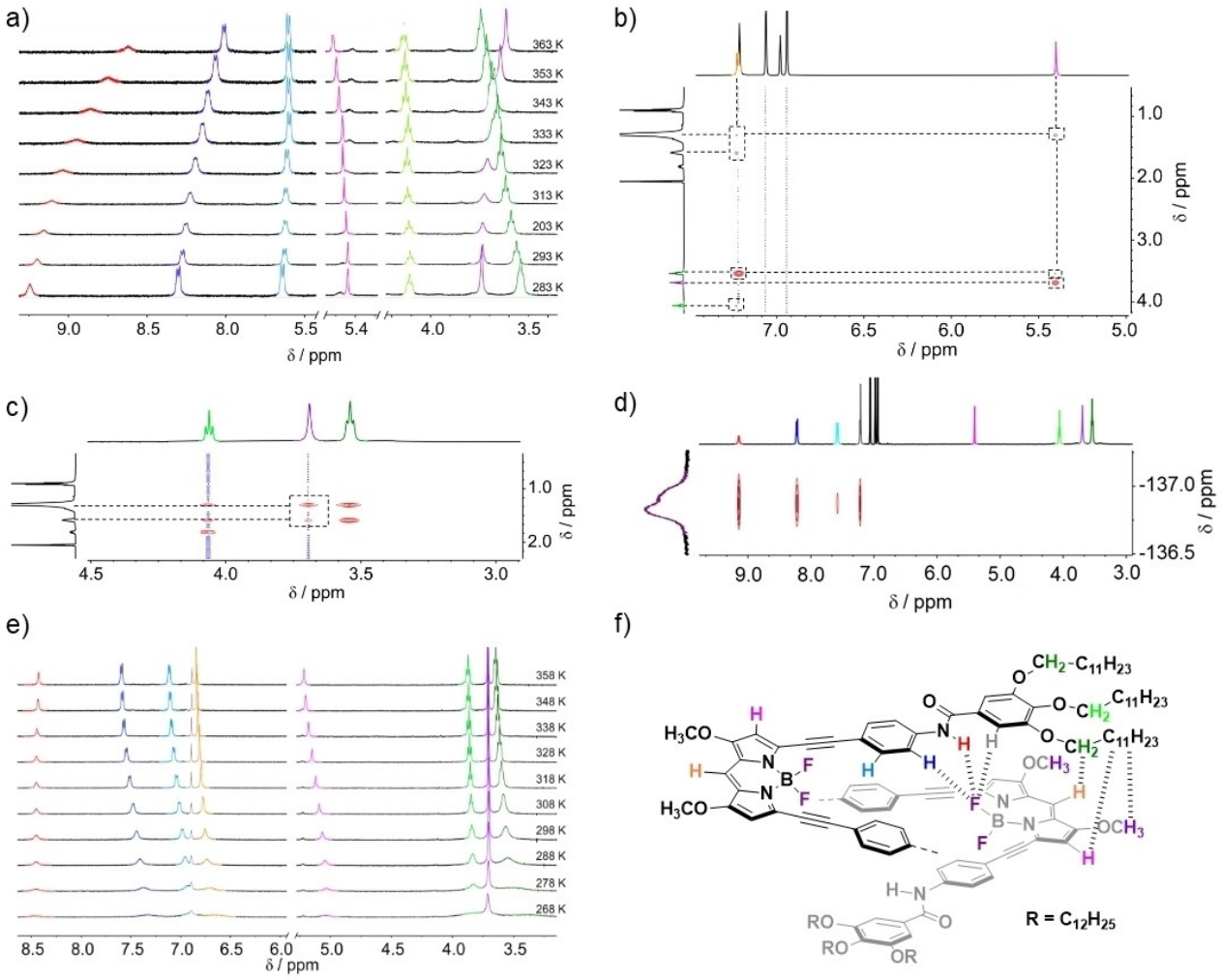

Figure 4. a) VT-^{1}H NMR spectra of **1** in toluene-d_8 (c = 1.8 mM); b) and c) partial 2D ROESY NMR spectrum of **1** in toluene-d_8 (c = 25 mM, T = 298 K); d) ^{1}H-^{19}F HOESY NMR spectrum of **1** in toluene-d_8 (c = 14 mM, T = 298 K); e) VT-^{1}H-NMR spectra of **1** in MCH-d_{14} (c = 2 mM); f) Proposed antiparallel molecular packing on the basis of NMR studies.

© 2023 The Authors. Angewandte Chemie International Edition published by Wiley-VCH GmbH

15213773, 2023, 17, Downloaded from https://onlinelibrary.wiley.com/doi/10.1002/anie.202218555 by Universidad De Burgos, Wiley Online Library on [07/02/2024]. See the Terms and Conditions (https://onlinelibrary.wiley.com/terms-and-conditions) on Wiley Online Library for rules of use; OA articles are governed by the applicable Creative Commons License

Additional insights into the molecular packing of **1** in toluene-d_8 were gained from 2D Rotating frame Overhauser Enhancement Spectroscopy (ROESY) NMR studies. Apart from various intramolecular interactions (see Figure S19), some key intermolecular interactions were also identified. The signal of the BODIPY *meso*-H (orange) shows a correlation with the O–C$\underline{H}_2$ groups of the outer dodecyloxy chains (dark green), as well as a very weak interaction with the O–C$\underline{H}_2$ group of the inner dodecyloxy chains (light green). Furthermore, the protons located at the 2- and 6-positions of the BODIPY core (pink) show a weak interaction with the O–$\underline{CH}_2$ groups of the outer dodecyloxy chains (dark green) and a clear correlation with the broad signal corresponding to the peripheral chains (Figure 4b). Likewise, the methoxy protons at the BODIPY core (purple) couple with most of the protons of the peripheral chains (Figure 4c). All observed correlation signals indicate spatial proximity between the BODIPY core and the peripheral dodecyloxy chains, which can only occur in an intermolecular fashion. Therefore, the BODIPY core of a monomer must necessarily be located in the vicinity of the trisubstituted benzamide ring of a neighboring monomer within the oligomer stack.

This proposed packing was ultimately demonstrated by ^{1}H-^{19}F-HOESY NMR experiments in toluene-d_8 (Figure 4d). Clear correlations between the amide N–H protons (red) and the $C_{aromatic}$-H protons of the neighboring aromatic rings (blue and gray signals) with the fluorine atoms are observed. This coupling pattern in combination with VT-^{1}H-NMR and ROESY studies clearly indicate the establishment of intermolecular B–F···H–N (amide) and various B–F···H–$C_{aromatic}$ interactions in the oligomer stacks in toluene, thus supporting an antiparallel-like molecular arrangement (Figure 4f). This packing is unambiguously supported by X-ray studies of parent BODIPY **4** with methoxy instead of dodecyloxy groups (Figure S30–S34, Tables S6, and S7).

Previously, we showed that the aggregates of **1** in MCH show a very high thermal stability and no disassembly into free monomers occurs even upon prolonged heating. The resulting absorption spectrum at high temperatures in MCH resembles that in toluene at room temperature, indicating that heating partially breaks some sort of secondary interactions—possibly involving solvation effects—but the core element of the oligomers is preserved. Thus, we attempted to examine these effects by analogous NMR studies in MCH-d_{14}. Note that a much higher concentration (3–4 orders of magnitude) is needed compared to UV/Vis, which further enhances aggregation. As expected, the spectrum of **1** in MCH-d_{14} at room temperature (298 K) and below (down to 268 K) shows a significant signal broadening (Figure 4e). Upon heating, an overall sharpening of the resonances is accompanied by a progressive downfield shift of the aromatic protons, indicating the partial rupture of π-π stacking interactions (Figure 4e). In contrast, the signals of the amide N–H protons showed no shifts upon cooling, even though previous FTIR studies under identical conditions revealed similar weak H-bonding interactions as those found in toluene. Based on these results and on the proven inability of **1** to dissociate into the monomers in MCH upon dilution and/or heating, we infer that VT-^{1}H-NMR studies only allow us to monitor the partial disruption of secondary interactions, e.g., aromatic, van der Waals and solvophobic, upon heating, but not the multiple types of H-bonding interactions.

Possibly, the oligomers in MCH are efficiently shielded by wrapping effects of the peripheral side chains, most likely enabling the effective intercalation of the solvent molecules into the chain shell.[23] This solvent intercalation along with stronger solvophobic effects enable closer distances between the aromatic backbones in the stack in MCH compared to toluene. Upon heating, partial desolvation of the alkoxy chains leads to a looser molecular packing, as suggested by the sharpening and deshielding of the aliphatic signals upon heating (Figure 4e).

Additionally, ^{1}H-^{19}F-HOESY and 2D ROESY NMR experiments in MCH-d_{14} (Figure S18 and S20) revealed a similar molecular packing as in toluene. In addition, the interdigitation of the alkoxy chains was observed, in good agreement with previous VT-^{1}H-NMR studies. With the information extracted from VT-^{1}H NMR, ROESY NMR and ^{1}H-^{19}F-HOESY NMR, the molecular packing of **1** could be elucidated. Considering the correlations between the BODIPY proton signals and those of the solubilizing alkoxy chains, an antiparallel molecular arrangement is proposed. In addition, the fluorine atoms of the BODIPY core of one monomer have to be spatially close to the amide N–H protons of neighboring monomers in order to successfully build H-bonds. On this basis, the BODIPY core must be necessarily located nearly on top of the outer phenyl ring. Furthermore, because the protons located at the 2- and 6-positions of the BODIPY only showed a weak correlation with the outer lateral chains, a displacement of the molecules is necessary to explain the experimental findings. As a consequence, the fluorine atoms of a BODIPY would interact with the amide protons of two different molecules, enabling the proposed staggered antiparallel arrangement shown in Figure 4f.

Theoretical calculations

Further insights into the self-assembly process were obtained by DFT calculations at the B3LYP/6-31G(d,p) level in gas phase. In order to reduce computational expenses, the dodecyloxy side chains were trimmed to methoxy groups. First, the geometries of different monomer conformations were fully optimized with the aim of obtaining the most stable conformer as the starting point for the optimization of oligomer species. The three optimized monomer conformations mainly differ in the orientation of the amide groups: both N–H groups pointing inwards, outwards, or in the same direction (Figure 5a and S52). Notably, the most stable conformation is the one with both N–H groups pointing in the same direction (one inwards and the other outwards), as this is the only orientation that enables an intramolecular N–H···O=C H-bond between the two amide groups of both arms of the BODIPY (distance N–H···O=C 2.14 Å) (Figure 5a). Two such monomers were subsequently stacked in

© 2023 The Authors. Angewandte Chemie International Edition published by Wiley-VCH GmbH

15213773, 2023, 17, Downloaded from https://onlinelibrary.wiley.com/doi/10.1002/anie.202218555 by Universidad De Burgos, Wiley Online Library on [07/02/2024]. See the Terms and Conditions (https://onlinelibrary.wiley.com/terms-and-conditions) on Wiley Online Library for rules of use; OA articles are governed by the applicable Creative Commons License

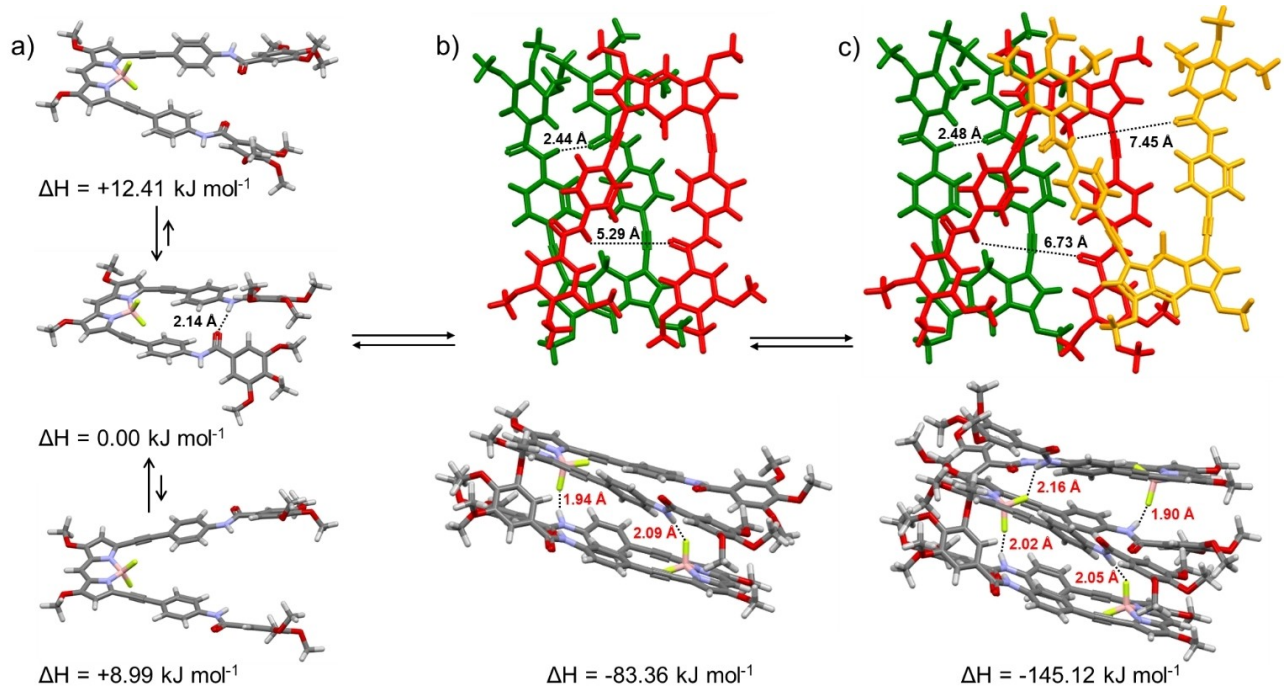

Figure 5. DFT optimized (supra)molecular structures obtained for the self-assembly process of **1** and calculated enthalpies at the B3LYP/6-31G(d,p) level in gas phase. a) Optimization of the V-shaped BODIPY monomer; b) Views of the optimized dimer showing the N–H···O=C (black) and N–H···F–B (red) bond lengths; c) Optimized trimer showing the N–H···O=C (black) and N–H···F–B (red) bond lengths.

an antiparallel fashion to optimize a dimer (Figure 5b). Interestingly, the dimer formation is accompanied by a structural change of the molecule: while the intramolecular N–H···O=C H-bonding interaction dissociates, two new intermolecular H-bonding interactions between the amide N–H and the fluorine atom of the BF_2 moiety are formed (distances N–H···F–B 1.94 and 2.09 Å) along with weaker interactions with the C–H groups at the aromatic *ortho* positions. These interactions promote an opening of the cleft defined by the BODIPY aromatic substituents, which becomes more evident when a third molecule is added to optimize a trimer (Figure 5c). Herein, the BF_2 unit of the central monomer forms N–H···F–B interactions with amide N–H groups of the molecules sitting above and below, leading to a triple decker staggered trimer with antiparallel molecular arrangement (Figure 5c). In turn, the amide N–H groups of the central monomer are engaged in interactions with the BF_2 moieties of the molecules sitting above and below (distances N–H···F–B 1.90–2.16 Å, Figure 5c). These interactions promote a further opening of the substituent's cleft upon stacking of the molecules, which may be an important factor contributing to the experimentally observed anticooperativity. This is also reflected by the fact that the dimerization is energetically more favorable than the trimerization (stabilization energy per monomer: dimer: $-83.36\ kJ\,mol^{-1}$; trimer: $-72.56\ kJ\,mol^{-1}$, Table S8). Additionally, we envisage that potential steric and enwrapping effects of the alkoxy chains (see previous ROESY NMR studies and schematic representation in Figure S18b,c), which were not included in the calculations, may also significantly contribute to limiting the oligomer growth.[8b]

Considering that V-shaped BODIPYs **2** and **3** lacking groups for H-bonding are unable to undergo efficient aggregation, we conclude that the C/N–H···F interactions characterizing **1** represent a sufficiently strong attractive force to counterbalance the molecular distortion and chain steric effects, ultimately enabling self-limiting growth at the stage of oligomers and contributing to their exceptionally high stability.

Conclusion

In conclusion, we have shown that the design of V-shaped monomer units is a powerful strategy towards anticooperatively formed discrete oligomeric assemblies. Notably, as a result of long distances between the BODIPY dyes within the aggregates, strong luminescence ($\Phi_f = 59\,\%$) is achieved in the oligomers. Comparison of the self-assembly of V-shaped BODIPY derivatives **1**–**3** additionally suggests that amide groups are essential to initiate the oligomerization process through establishment of unconventional C/N–H···F–B intermolecular interactions. Without these hydrogen bonding interactions, the distorted V-shaped molecular core and additional steric effects of the side chains dominate and no aggregation takes place. Proof of this is the negligible aggregation of **2** and **3** (which lack amide groups) compared to **1** under similar conditions. While **1** forms discrete oligomers in both toluene and methylcyclohexane,

© 2023 The Authors. Angewandte Chemie International Edition published by Wiley-VCH GmbH

15213773, 2023, 17, Downloaded from https://onlinelibrary.wiley.com/doi/10.1002/anie.202218555 by Universidad De Burgos, Wiley Online Library on [07/02/2024]. See the Terms and Conditions (https://onlinelibrary.wiley.com/terms-and-conditions) on Wiley Online Library for rules of use; OA articles are governed by the applicable Creative Commons License

the monomer-oligomer equilibrium in toluene is not shifted to the oligomer side, possibly as a result of weak aromatic interactions and less efficient side chain solvation and enwrapping effects. Notably, this latter effect becomes highly dominant in methylcyclohexane, which in combination with C/N–H···F interactions, stabilize the discrete oligomers of **1** to the point that no thermal disassembly takes place, not even after prolonged heating or dilution. Our results broaden the monomer scope for anticooperative supramolecular polymerizations. Additionally, the self-limiting growth and the remarkable NIR-luminescence of these assemblies represents a sound basis for the development of novel optoelectronic and bio-materials.

Acknowledgements

We thank the Deutsche Forschungsgemeinschaft (SFB858) for funding (B.M. and G.F.). B.S. thanks the MICINN/AEI of Spain for the projects EQC2018-004206-P, RED2018-102331-T, PID2019-107779GA-I00/AEI/10.13039/501100011033 and RYC-2017-21789. M. G.-V. and R.Q. thank funding from Consejería de Educación de la Junta de Castilla y León and ERDF (project BU067P20) and MICN/AEI/10.13039/501100011033 (grant PID2020-117610RB-100). S.D.-C. and I.C.-B. thank Consejería de Educación de la Junta de Castilla y León, ERDF (European Regional Development Fund) and European Social Fund for their pre- and post-doctoral contracts, respectively.Conflict of Interest Open Access funding enabled and organized by Projekt DEAL.

The authors declare no conflict of interest.

Data Availability Statement

The data that support the findings of this study are available in the Supporting Information of this article.

Keywords: Anticooperativity · BODIPY Dyes · Hydrogen Bonding · Self-Assembly · Supramolecular Polymerization

[1] a) M. H.-Y. Chan, V. W.-W. Yam, *J. Am. Chem. Soc.* **2022**, *144*, 22805–22825; b) G. Ghosh, T. Ghosh, G. Fernández, *ChemPlusChem* **2020**, *85*, 1022–1033; c) G. Ghosh, P. Dey, S. Ghosh, *Chem. Commun.* **2020**, *56*, 6757–6769; d) M. Wehner, F. Würthner, *Nat. Chem. Rev.* **2020**, *4*, 38–53; e) Y. Han, Z. Gao, C. Wang, R. Zhong, F. Wang, *Coord. Chem. Rev.* **2020**, *414*, 213300; f) J. Matern, Y. Dorca, L. Sánchez, G. Fernández, *Angew. Chem. Int. Ed.* **2019**, *58*, 16730–16740; *Angew. Chem.* **2019**, *131*, 16884–16895; g) S. Dhiman, S. George, *Bull. Chem. Soc. Jpn.* **2018**, *91*, 687–699; h) T. Aida, E. W. Meijer, *Isr. J. Chem.* **2020**, *60*, 33–47; i) P. A. Korevaar, T. F. A. de Greef, E. W. Meijer, *Chem. Mater.* **2014**, *26*, 576–586.

[2] a) F. Würthner, C. R. Saha-Möller, B. Fimmel, S. Ogi, P. Leowanawat, D. Schmidt, *Chem. Rev.* **2016**, *116*, 962–1052; b) S. S. Babu, V. K. Praveen, A. Ajayaghosh, *Chem. Rev.* **2014**, *114*, 1973–2129; c) S. S. Babu, K. K. Kartha, A. Ajayaghosh, *J. Phys. Chem. Lett.* **2010**, *1*, 3413–3424; d) F. J. M. Hoeben, P. Jonkheijm, E. W. Meijer, A. P. H. J. Schenning, *Chem. Rev.* **2005**, *105*, 1491–1546.

[3] a) S. Yagai, Y. Kitamoto, S. Datta, B. Adhikari, *Acc. Chem. Res.* **2019**, *52*, 1325–1335; b) Y. Dorca, E. E. Greciano, J. S. Valera, R. Gómez, L. Sánchez, *Chem. Eur. J.* **2019**, *25*, 5848–5864; c) A. Sikder, S. Ghosh, *Mater. Chem. Front.* **2019**, *3*, 2602–2616; d) A. Das, S. Ghosh, *Chem. Commun.* **2016**, *52*, 6860–6872; e) D. González-Rodríguez, A. P. H. J. Schenning, *Chem. Mater.* **2011**, *23*, 310–325.

[4] a) C. Kulkarni, E. W. Meijer, A. R. A. Palmans, *Acc. Chem. Res.* **2017**, *50*, 1928–1936; b) C. Rest, R. Kandanelli, G. Fernández, *Chem. Soc. Rev.* **2015**, *44*, 2543–2572; c) C. Kulkarni, S. Balasubramanian, S. J. George, *ChemPhysChem* **2013**, *14*, 661–673.

[5] M. F. Hagan, G. M. Grason, *Rev. Mod. Phys.* **2021**, *93*, 25008.

[6] T. F. A. de Greef, M. M. J. Smulders, M. Wolffs, A. P. H. J. Schenning, R. P. Sijbesma, E. W. Meijer, *Chem. Rev.* **2009**, *109*, 5687–5754.

[7] a) W. Shi, R. Wei, D. Zhang, L. Meng, J. Xie, K. Cai, D. Zhao, *Angew. Chem. Int. Ed.* **2022**, *61*, e2022086; *Angew. Chem.* **2022**, *134*, e2022086; b) Y. Vonhausen, A. Lohr, M. Stolte, F. Würthner, *Chem. Sci.* **2021**, *12*, 12302–12314; c) R. Renner, M. Stolte, F. Würthner, *ChemistryOpen* **2020**, *9*, 32–39; d) J. Gershberg, F. Fennel, T. H. Rehm, S. Lochbrunner, F. Würthner, *Chem. Sci.* **2016**, *7*, 1729–1737; e) R. van der Weegen, P. A. Korevaar, P. Voudouris, I. K. Voets, T. F. A. de Greef, J. A. J. M. Vekemans, E. W. Meijer, *Chem. Commun.* **2013**, *49*, 5532–5534.

[8] a) I. Helmers, M. Saddam Hossain, N. Bäumer, P. Wesarg, B. Soberats, L. S. Shimizu, G. Fernández, *Angew. Chem. Int. Ed.* **2022**, *61*, e202200390; *Angew. Chem.* **2022**, *134*, e202200390; b) Y. Dorca, C. Naranjo, G. Ghosh, B. Soberats, J. Calbo, E. Ortí, G. Fernández, L. Sánchez, *Chem. Sci.* **2022**, *13*, 81–89; c) L. Herkert, J. Droste, K. K. Kartha, P. A. Korevaar, T. F. A. de Greef, M. R. Hansen, G. Fernández, *Angew. Chem. Int. Ed.* **2019**, *58*, 11344–11349; *Angew. Chem.* **2019**, *131*, 11466–11471; d) F. Su, G. Chen, P. A. Korevaar, F. Pan, H. Liu, Z. Guo, A. P. H. J. Schenning, H.-J. Zhang, J. Lin, Y.-B. Jiang, *Angew. Chem. Int. Ed.* **2019**, *58*, 15273–15277; *Angew. Chem.* **2019**, *131*, 15417–15421; e) P. P. N. Syamala, B. Soberats, D. Görl, S. Gekle, F. Würthner, *Chem. Sci.* **2019**, *10*, 9358–9366; f) K. Cai, J. Xie, D. Zhang, W. Shi, Q. Yan, D. Zhao, *J. Am. Chem. Soc.* **2018**, *140*, 5764–5773; g) R. Appel, J. Fuchs, S. M. Tyrrell, P. A. Korevaar, M. C. A. Stuart, I. K. Voets, M. Schönhoff, P. Besenius, *Chem. Eur. J.* **2015**, *21*, 19257–19264; h) A. Arnaud, J. Belleney, F. Boué, L. Bouteiller, G. Carrot, V. Wintgens, *Angew. Chem. Int. Ed.* **2004**, *43*, 1718–1721; *Angew. Chem.* **2004**, *116*, 1750–1753; i) X. Li, L. E. Sinks, B. Rybtchinski, M. R. Wasilewski, *J. Am. Chem. Soc.* **2004**, *126*, 10810–10811; j) E. R. Zubarev, M. U. Pralle, L. Li, S. I. Stupp, *Science* **1999**, *283*, 523–526.

[9] a) P. Besenius, G. Portale, P. H. H. Bomans, H. M. Janssen, A. R. A. Palmans, E. W. Meijer, *Proc. Natl. Acad. Sci. USA* **2010**, *107*, 17888–17893; b) H. Dong, S. E. Paramonov, L. Aulisa, E. L. Bakota, J. D. Hartgerink, *J. Am. Chem. Soc.* **2007**, *129*, 12468–12472.

[10] B. Matarranz, G. Ghosh, R. Kandanelli, A. Sampedro, K. K. Kartha, G. Fernández, *Chem. Commun.* **2021**, *57*, 4890–4893.

[11] a) S. Bujosa, A. Doncel-Giménez, N. Bäumer, G. Fernández, E. Ortí, A. Costa, C. Rotger, J. Aragó, B. Soberats, *Angew. Chem. Int. Ed.* **2022**, *61*, e202213345; *Angew. Chem.* **2022**, *134*, e202213345; b) I. Helmers, N. Bäumer, G. Fernández, *Chem.*

© 2023 The Authors. Angewandte Chemie International Edition published by Wiley-VCH GmbH

15213773, 2023, 17, Downloaded from https://onlinelibrary.wiley.com/doi/10.1002/anie.202218555 by Universidad De Burgos, Wiley Online Library on [07/02/2024]. See the Terms and Conditions (https://onlinelibrary.wiley.com/terms-and-conditions) on Wiley Online Library for rules of use; OA articles are governed by the applicable Creative Commons License

Commun. **2020**, *56*, 13808–13811; c) T. Fukui, S. Kawai, S. Fujinuma, Y. Matsushita, T. Yasuda, T. Sakurai, S. Seki, M. Takeuchi, K. Sugiyasu, *Nat. Chem.* **2017**, *9*, 493–499; d) S. Ghosh, X.-Q. Li, V. Stepanenko, F. Würthner, *Chem. Eur. J.* **2008**, *14*, 11343–11357.

[12] a) J. Li, Q. Zhang, J. Yin, C. Yu, K. Cheng, Y. Wei, E. Hao, L. Jiao, *Org. Lett.* **2016**, *18*, 5696–5699; b) M. R. Rao, M. D. Tiwari, J. R. Bellare, M. J. Ravikanth, *Org. Chem.* **2011**, *76*, 7263–7268; c) A. Fürstner, *Angew. Chem. Int. Ed.* **2003**, *42*, 3582–3603; *Angew. Chem.* **2003**, *115*, 3706–3728; d) J. W. Bennett, R. Bentley, *Adv. Appl. Microbiol.* **2000**, *47*, 1–32.

[13] a) B. Matarranz, G. Fernández, *Chem. Phys. Rev.* **2021**, *2*, 041304; b) S. Cherumukkil, B. Vedhanarayanan, G. Das, V. K. Praveen, A. Ajayaghosh, *Bull. Chem. Soc. Jpn.* **2018**, *91*, 100–120.

[14] a) N. J. Hestand, F. C. Spano, *Chem. Rev.* **2018**, *118*, 7069–7163; For recent examples of BODIPY J-aggregates, see: b) X. Wang, Z. Jiang, Z. Liang, T. Wang, Y. Chen, Z. Liu, *Sci. Adv.* **2022**, *8*, eadd5660; c) K. Li, X. Duan, Z. Jiang, D. Ding, Y. Chen, G. Q. Zhang, Z. Liu, *Nat. Commun.* **2021**, *12*, 2376; d) Y. Zhang, S. Yuan, P. Liu, L. Jing, H. Pan, X.-K. Ren, Z. Chen, *Org. Chem. Front.* **2021**, *8*, 4078–4085; e) Y. Zhang, P. Liu, H. Pan, H. Dai, X.-K. Ren, Z. Chen, *Chem. Commun.* **2020**, *56*, 12069–12072.

[15] M. M. J. Smulders, M. M. L. Nieuwenhuizen, T. F. A. de Greef, P. van der Schoot, A. P. H. J. Schenning, E. W. Meijer, *Chem. Eur. J.* **2010**, *16*, 362–367.

[16] P. A. Korevaar, C. Schaefer, T. F. A. de Greef, E. W. Meijer, *J. Am. Chem. Soc.* **2012**, *134*, 13482–13491.

[17] R. F. Goldstein, L. Stryer, *Biophys. J.* **1986**, *50*, 583–599.

[18] a) G. Das, S. Cherumukkil, A. Padmakumar, V. B. Banakar, V. K. Praveen, A. Ajayaghosh, *Angew. Chem. Int. Ed.* **2021**, *60*, 7851–7859; *Angew. Chem.* **2021**, *133*, 7930–7938; b) J. Matern, K. K. Kartha, L. Sánchez, G. Fernández, *Chem. Sci.* **2020**, *11*, 6780–6788; c) E. E. Greciano, S. Alsina, G. Ghosh, G. Fernández, L. Sánchez, *Small Methods* **2020**, *4*, 1900715.

[19] a) A. Langenstroer, K. K. Kartha, Y. Dorca, J. Droste, V. Stepanenko, R. Q. Albuquerque, M. R. Hansen, L. Sánchez, G. Fernández, *J. Am. Chem. Soc.* **2019**, *141*, 5192–5200.

[20] a) J. S. Valera, J. Calbo, R. Gómez, E. Ortí, L. Sánchez, *Chem. Commun.* **2015**, *51*, 10142–10145; b) F. García, L. Sánchez, *J. Am. Chem. Soc.* **2012**, *134*, 734–742.

[21] S. Cherumukkil, S. Ghosh, V. K. Praveen, A. Ajayaghosh, *Chem. Sci.* **2017**, *8*, 5644–5649.

[22] The observation of relatively sharp NMR signals for the aggregate of **1** in -toluene-d_8 may either suggest that the SAXS results slightly overestimate the oligomer size, and/or the presence of free monomers in equilibrium with the oligomer assemblies under these conditions.

[23] C. Kulkarni, P. A. Korevaar, K. K. Bejagam, A. R. A. Palmans, E. W. Meijer, S. J. George, *J. Am. Chem. Soc.* **2017**, *139*, 13867–13875.

Manuscript received: December 15, 2022
Accepted manuscript online: February 24, 2023
Version of record online: March 16, 2023

© 2023 The Authors. Angewandte Chemie International Edition published by Wiley-VCH GmbH

15213773, 2023, 17, Downloaded from https://onlinelibrary.wiley.com/doi/10.1002/anie.202218555 by Universidad De Burgos, Wiley Online Library on [07/02/2024]. See the Terms and Conditions (https://onlinelibrary.wiley.com/terms-and-conditions) on Wiley Online Library for rules of use; OA articles are governed by the applicable Creative Commons License